# Porous Functionalized Polymers enable Generating and Transporting Hyperpolarized Arbitrary Solutions.

**Théo El Darai**
Univ. Lyon, CNRS - Centre de RMN à Très Hauts Champs de Lyon, FRE2034
**Samuel Cousin**
Univ. Lyon, CNRS - Centre de RMN à Très Hauts Champs de Lyon, FRE2034
**Quentin Chappuis**
Univ. Lyon, CNRS - Centre de RMN à Très Hauts Champs de Lyon, FRE2034
**Morgan Ceillier**
Univ. Lyon, CNRS - Centre de RMN à Très Hauts Champs de Lyon, FRE2034
**James Kempf**
Bruker Biospin, Billerica, Massachusetts 01821, United States
**Dmitry Eshchenko**
Bruker Biospin, 8117 Fallanden, Switzerland
**Roberto Melzi**
Bruker Italia Srl, 20158 Milano, Italy
**Marc Schnell**
Bruker Biospin, 8117 Fallanden, Switzerland
**Laurent Gremillard**
Univ Lyon, INSA Lyon, MATEIS UMR CNRS 5510 https://orcid.org/0000-0001-7258-6483
**Aurélien Bornet**
Ecole Polytechnique Fédérale de Lausanne
**Jonas Milani**
Univ. Lyon, Centre de RMN à Très Hauts Champs de Lyon, FRE2034
**Basile Vuichoud**
Univ. Lyon, Centre de RMN à Très Hauts Champs de Lyon, FRE2034
**Olivier Cala**
Univ. Lyon, Centre de RMN à Très Hauts Champs de Lyon, FRE2034
**Damien Montarnal** (✉ damien.montarnal@univ-lyon1.fr)
CNRS, Univ. Lyon https://orcid.org/0000-0003-3246-3467
**Sami Jannin**
Université Claude Bernard Lyon 1 https://orcid.org/0000-0002-8877-4929

**Article**

**Keywords:** Hyperpolarization, dissolution dynamic nuclear polarization, hyperpolarizing polymers

**Posted Date:** January 14th, 2021

**DOI:** https://doi.org/10.21203/rs.3.rs-123790/v1



**Version of Record:** A version of this preprint was published at Nature Communications on August 4th, 2021. See the published version at https://doi.org/10.1038/s41467-021-24279-2.

# Abstract

Hyperpolarization by dissolution dynamic nuclear polarization (dDNP) has brought highly sensitive magnetic resonance to reality and has triggered the development of a plethora of promising applications in spectroscopy and imaging. Unfortunately, some severe limitations still restrain its widespread use, amongst which the experimental complexity, the need for trained personnel, and excessive prices. Broad democratization of dDNP would require remote preparation of hyperpolarized samples in dedicated facilities and transport over long distances to the point of use. We have recently pioneered a new concept in which transport over hours was enabled by formulation of 13C-labelled molecules into micro-crystallites. However, the proposed methods lacked both versatility and biocompatibility. Here, we propose a new approach relying on a new generation of hyperpolarizing polymers (HYPOPs), extremely easy to synthesize, and that bear a dual function. Arbitrary solutions, easily impregnated into these radical-containing porous HYPOPs, can be hyperpolarized within 20 min with a polarization level exceeding P(13C) > 25% in the solid state, and further stored for hours in view of transport to a remote point of use.


# Introduction

Nuclear magnetic resonance (NMR) and magnetic resonance imaging (MRI) have become, within 50 years, techniques of reference for both analytical chemistry and medical diagnostic. The development of very high magnetic fields has led to an incessant increase in resolution and sensitivity which has enabled faster acquisitions at ever decreasing concentrations. However, sensitivity still remains the Achilles Heel of magnetic resonance. Today, the development of hyperpolarization methods to further enhance sensitivity by large factors is one of the most important topics of research in magnetic resonance.

Dissolution dynamic nuclear polarization (dDNP) is one of these hyperpolarization game-changing approaches applicable for both NMR and MRI. dDNP enables hyperpolarization of small molecules therefore spectacularly amplifying their magnetic resonance signals by up to four orders of magnitude.[1,2] Such hyperpolarization is typically carried out in a dedicated apparatus (a dDNP polarizer) and harsh conditions (high magnetic field, extreme cryogenic temperatures) where the close to unity electron-spin alignment of polarizing agents (PAs, typically molecules containing unpaired electrons) is transferred to the nuclear spins ($^{1}$H, $^{13}$C, $^{31}$P, $^{15}$N etc.) of target molecules. Despite promising proofs of concepts such as the detection of intermediates in fast chemical reactions,[3] the observation of protein folding in real time,[4] or the early detection and monitoring of tumors in humans,[5] dDNP remains unfortunately restricted to a small number of specialized research groups around the globe. Indeed, some severe limitations restrain the widespread use of the method, amongst which the experimental complexity involving sterility (for clinical studies[6]), extreme cryogenic temperatures (1.2 <T <4.2 K), high magnetic fields (up to $B_0$ = 9 T[7]), and microwave irradiation sometimes coupled to synchronized radiofrequency irradiation.[8,9] It also requires trained personnel, and finally represents an overall excessive price for the equipment and cryogenic fluids.

Most of these issues would be virtually fixed from the user perspective if one could transport hyperpolarized molecules from a large-scale hyperpolarization preparation centre to the end users' remote locations. In a word, one would need to turn hyperpolarization into a long-lived transportable *consumable*, thus alleviating the struggle of local preparation. Unfortunately, the short-lived character of hyperpolarization in solution (on the order of a minute apart from some exotic cases[10,11] and long-lived states[12–15]), requires that the complex dDNP preparation of the hyperpolarized samples be performed "on-site", next to the NMR or MRI machine.

This fundamental drawback arises from the very nature of dDNP sample formulations featuring an intimate contact of a few nanometres between target molecules (typically $^{13}$C labelled metabolites) and paramagnetic PAs (which has for a long time thought to be necessary for efficient hyperpolarization). Therefore, the PAs and the target molecule are usually homogeneously mixed then shock-frozen in a glassy state. Such rapid freezing ensures a statistical distribution of both components[16,17]. Yet, this close proximity also leads to paramagnetic nuclear spin relaxation induced by electron spin flip-flops of the PAs,[18–21] which causes complete hyperpolarization loss within milliseconds (in solids)[22] to seconds (in liquids) when the sample is removed from magnetic field of the polarizer and its cryogenic environment.

One promising answer to this roadblock relies on non-persistent PAs such as photo-excited triplets[23] or photogenerated radicals.[24–26] We have recently introduced another approach that deliberately avoids intimate mixing of the target molecules and PAs through phase separation. In this previous work,[27] we designed a dDNP sample formulation in which the $^{13}$ C-labelled target molecules were provided in the form of microcrystals (typically 1-10 µm large) dispersed in an organic phase (for example toluene/THF) containing the PAs. While direct hyperpolarization of $^{13}$C may appear impossible at first sight in such sample formulations given the long distances (several µm) between $^{13}$C nuclear spins and PAs, the $^{1}$H abundance in the two phases enables an indirect three-step polarization procedure:

i. microwave irradiation rapidly builds $^{1}$H polarization in the solvent near the PAs
ii. this $^{1}$H spin polarization spontaneously diffuses to the $^{1}$H spins within the micro-crystals.
iii. The $^{1}$H spin polarization is then transferred to the $^{13}$C spins of the target molecule by irreversible $^{1}$H→$^{13}$C cross-polarization[28,29] (CP).

This new method offered hyperpolarization lifetimes exceeding tens of hours on some $^{13}$ C-labelled target molecules, thus enabling the transport and storage of hyperpolarized molecules at 4.2 K. This method is, however, restricted to small molecules amenable to well-tailored micro-crystals and involves poisonous organic solvents along with PA residues, which precludes its use with proteins, living cells or animals.

A definitive answer to this issue would be to find a way to generalize the phase-separation strategy to arbitrary sample formulations (molecules, mixtures, biological fluids, etc.) without the use of any

contaminants (such as the organic solvents hosting the PAs). This would have the potential to transform and democratize the benefits of hyperpolarization to a very wide NMR and MRI community. Target molecules could be hyperpolarized in dedicated centers and delivered as “consumables” ready for dissolution and injection to NMR or MRI.

To achieve such goal, we propose a new strategy where PAs are covalently bound within a macro-porous and monolithic polymer scaffold, acting as an immiscible stationary phase, in which aqueous solutions of target molecules (such as of $^{13}$C-labelled metabolites) are loaded by incipient wetness impregnation (IWI). The porous polymer scaffolds are straightforwardly synthesized from commercial epoxy formulations and a non-reactive solvent, thanks to thorough investigation of the spinodal decomposition occurring during the curing reaction. Previous generations of polarizing materials for dDNP involved surface grafted nitroxides (HYPSO,[30,31] FLAP,[32] hydrogels[33]), that prevented hyperpolarization transport. Here the specificity of our new generation of hyperpolarizing polymers (HYPOP) lies in an increased and tailored separation between the PAs and the target molecules that enable hyperpolarization transport by (i) featuring characteristic separation length from the target molecules (above. 100 nm) considerably larger than for previous HYPSO material (c.a. 6 nm), and (ii) locating the PAs deep in the bulk of the polymer and not only at the porous surface.

In this article, we show how HYPOPs are specifically synthesized and tailored with a simple protocol in order to meet all the requirements for optimal dDNP performances. First, these polymers must withstand extreme cryogenic temperatures (down to superfluid helium at 1.2 K) but also very fast temperature jumps from 1.2 K to ca. 350 K when extracting the hyperpolarized vitrified solution with superheated water in less than a second. The second requirement is of a chemical nature: these polymers should be easily functionalized with stable radical molecules, such as TEMPO derivatives, and at various concentrations. Indeed, optimal concentrations of TEMPO species for dDNP were previously determined at around 50-100 µmol/g in a variety of systems.[34] The third requirement concerns the structure of the porous network, which must featurea high-volume fraction of open pores (ideally>75%) to maximize the quantity of target solution and an adjustable separation length between the TEMPO radicals and the target solution, determined by the aggregated polymer particles forming the network.

Strong levels of polarization for the impregnated arbitrary frozen solutions, exceeding $P(^{13}C)$> 25%, were achieved within tens of minutes under dDNP conditions,[9,35,36] and subsequently demonstrated a very slow relaxation $T_1$ above 5 hours at liquid helium temperature. Owing to the suitable surface energy of the epoxy resin chosen, pure hyperpolarized solutions can be remarkably well extracted from the HYPOPs, directly available for NMR and MRI injection at the point of use.

# Results And Discussion

**Hyperpolarization of arbitrary solutions using HYPOP; an overview.** Fig. 1 illustrates how HYPOPs can be used to hyperpolarize arbitrary solutions. We describe here a first generation of HYPOP materials dubbed HYPOPs-**I** that feature ca. 100 nm-large aggregated polymer particles forming a monolithic material with

open porosity (Fig. 1a). HYPOP-**I** can be impregnated (Fig. 1b) with a variety of liquids ranging from pure pyruvic acid (the gold standard in hyperpolarized metabolic imaging[5]) to complex aqueous solutions, such as mixtures of ligands for fragment-based drug discovery,[37] or mixtures of metabolites originating from cell extracts.[38] The $^{1}$H spins of the whole sample are polarized in c.a. 20 min to very high levels exceeding $P(^{1}H)$> 60%. This polarization originates from the aggregated epoxy particles of HYPOP-**I** in which PAs are hosted, and spontaneously propagates to the frozen solution by $^{1}$H nuclear spin diffusion.[39] This high $^{1}$H polarization is sheltered on low-gamma $^{13}$C nuclear spins of target molecules after brief cross-polarization contacts of a few milliseconds.[9] High levels of $^{13}$C polarization exceeding $P(^{13}C)$> 30% can thus be achieved in tens of minutes (represented in fig. 1d), and further stored at low temperatures (3.8 K) for hours in view of transport to a remote point of use (represented in Fig. 1e). The very long $^{13}$C relaxation times (up to 5.7 h) are attributed to the fact that paramagnetic relaxation is dramatically attenuated in the pores since $^{13}$C-$^{13}$C nuclear spin diffusion towards the paramagnetic PAs is orders of magnitude slower than for $^{1}$H, and further attenuated by the low natural abundance of $^{13}$C in the HYPOP-**I** material. We finally show how the hyperpolarized solutions can be extracted from HYPOP-**I** with high efficiency leading to hyperpolarized solution of metabolites that show exceptional signal enhancements upon immediate analysis with $^{13}$C NMR (Fig. 1f).

**HYPOP synthesis and characterization.** A considerable number of strategies can lead to polymer networks with open porosity of various sizes,[40,41] such as selective degradation of block copolymers assembled in co-continuous morphologies,[42] high internal phase emulsions (HIPE),[43] colloid templating,[44] aerogels or open-cell foams.[45] These methods also share some of the following shortcomings: i) synthetic complexity or incompatibility of polymerization strategies with the presence of stable radicals; ii) presence of additives in the materials such as surfactants; or iii) high temperature or chemical treatments incompatible with the survival of the TEMPO radicals. Other strategies, often applied to the synthesis of polymer membranes involve spinodal decomposition between a polymer and solvents through thermal transitions or changes in the solvent composition.[46] The porous network can then be obtained through straightforward removal of the solvents, but often displays significant heterogeneities. We rather opted for an analogous method, where spinodal decomposition between the polymer and the solvent is caused by the polymerization process itself. This process is also relatively easy to implement using thermosetting polymers with outstanding thermo-mechanical properties such as epoxy resins. Formulations of epoxy resin, hardener and a non-reactive solvent that display initially full miscibility, and that undergoes phase separation during the curing have been previously studied to form either epoxy materials as dispersed particles,[47] solids with closed porosity,[48,49] and also solids with open porosities.[50]

Thanks to a thorough study of the formulation (nature of the non-reactive solvent and relative fraction to the epoxy resin precursors), we were able to construct an extensive phase diagram of such a system and to target network morphologies in close adequacy with our requirements. We selected conventional epoxy resin precursors leading to high $T_g$ thermosets above 150 °C: diglycidyl ether of bisphenol A (DGEBA) and isophorone diamine (IPDA) (Fig. 2a). The mixture was cured at 373K during 24 h in presence of

polypropylene glycols (PPGs) of different molar mass acting as non-reactive solvents (detailed synthesis in the “methods” section). Thorough variations of the fraction of non-reactive solvents (from 30 to 90 wt %) and of their molar mass (from 192 to 2000 g $mol^{-1}$) have been tested in absence of 4-amino-TEMPO ($n$ = 0). This results in the formation of epoxy particles aggregated in a variety of morphologies such as stable latexes, unstable suspensions, gels, monolithic networks with closed and opened porosities. The corresponding phase diagram, presented in fig. 2b, was built from a series of experiments (each dot) and the nature of porosity, opened or closed, was assessed by gravimetry after extraction of the PPG. The functionalization of this resin with commercially available 4-amino-TEMPO is straightforward and was obtained by merely mixing this commercial TEMPO derivative with IPDA in various molar ratios; the amount of DGEBA was adjusted to maintain a proper stoichiometry between amines and epoxydes ($n_{epoxy}/n_{NH2}$ = 2). Solid samples were characterized, after proper removal of PPG using solvent washes and freeze-drying, by SEM, $N_2$ physisorption and Hg intrusion porosimetry when appropriate. All experimental details are given in the methods section and in the section 2 in the SI.

Spinodal decomposition leading to bicontinuous and homogeneous morphologies, and thus to solids with open porosity after extraction of the PPG, occurred only in a narrow range of solvent fractions (60-90 wt%), and for low molar mass of PPG. The corresponding size of aggregated epoxy particles was critically dependent on the molar mass of PPG, and varied from 1-5 µm, 100 nm and ca. 10 nm for PPG-725, PPG-400 and PPG-192, respectively (See Section 2.3 in the SI). The latter networks were obtained as transparent gels (i.e. not demonstrating extended phase separation between the epoxy and the solvent) and display structures typical of aerogels. Thus, the morphologies of the sample obtained with 85 wt% of PPG-400, showing a bicontinuous morphology composed of ca. 100 nm-large aggregated epoxy particles forming a solid with hierarchical porosity, was particularly well suited to our requirements, with a $T_g$ estimated to be 134 °C and the absence of fracture when immersed in liquid $N_2$. The proper curing of this particular network was monitored with in-situ rheology (Section 2.5 in SI) that enabled the identification of a first phase separation event after 3 h of reaction, followed 30 min later by the formation of a network between aggregated particles. As the storage modulus reached a plateau after about 15 h of reaction, we kept a curing time of 24 h for all samples. After subsequent extraction of the PPG and drying of the porous polymers, we found that the final weights of the solids are, within experimental error, the same as the epoxy-amine precursors. In addition, swelling tests indicate the complete absence of a soluble fraction and therefore a complete cross-linking process.

The epoxy formulation using 85 wt% of PPG-400 was modified with increasing amounts of 4-amino-TEMPO (with r = $n_{TEMPO\text{-}NH2}/n_{IPDA}$ ranging from 0 to 1.06) to obtain a series of seven HYPOP-**I** samples that are further used for the dDNP experiments. In spite of previous results indicating complete reaction of epoxides and amines, the concentration of radicals present in the final materials cannot be directly estimated from the initial amount of 4-aminoTEMPO and was measured by Electron Paramagnetic Resonance EPR (See section 3 in SI). By comparing the effective concentrations of radicals to the concentration of 4-aminoTEMPO initially added (Table S2 in SI), we found a fairly constant and reproducible survival yield of 34 % (free radicals surviving the synthesis). This value, seemingly low, was

to be expected from the long curing times (24 H) at 100 °C. This low rate is, however, acceptable in the HYPOP-**I** series given a) the relatively low cost of precursors and the simplicity of the synthesis and b) the large range of radical concentrations that are still attainable, up to 285 µmol $g^{-1}$, which goes beyond optimal concentrations required for dDNP (see below). Incorporating such large amounts of 4-aminoTEMPO in the epoxy networks in place of the tetra-functional IPDA can yet induce significant changes in the final materials morphology due to i) the decrease of both cross-link density and $T_g$ in the epoxy network and ii) changes of solubility parameters between epoxy and PPG that govern the spinodal decomposition and the final morphology of the materials. While an inspection of the HYPOP-**I** series with SEM (Section 2.4 in SI) hardly displays evidence of variations in the morphology, a more thorough analysis involving mercury intrusion porosimetry indicates noteworthy changes in the pore size distribution (Section 2.6 in SI). While all samples display similar distribution of pore sizes in the 10-100 nm range, i.e. within the interstices of the epoxy particles, micrometric pores corresponding to voids between particle aggregates are progressively disappearing when the amount of 4-amino-TEMPO is increased. Concomitantly, the total porous volume decreases from about 3.5 to 1 mL $g^{-1}$. We believe this to be due to an increased compatibility of the TEMPO-rich epoxy with the PPG, and thus a more extensive plasticization and susceptibility to pore collapse upon removal of the solvent. Complementary analyses with nitrogen physisorption (Fig. S4 in SI) also confirm that these networks are essentially macroporous, with pore sizes above 50 nm.

**HYPOP impregnation with aqueous solutions.** While HYPOP-**I** samples could be completely backfilled by immersion in a few centimetres of water or aqueous solutions, their low surface energy does not allow for spontaneous capillary impregnation. We resorted to use water/ethanol mixtures (9/1 v/v) for all impregnating solutions to circumvent this issue. Swelling of the HYPOP matrix is another important parameter to consider that could affect the PA concentration either by scavenging the radical[51], or simply by increasing the volume of the polymer and therefore decreasing the radical concentration and the dynamics of polarization. While a few organic solvents demonstrated extensive swelling, the water : ethanol mixtures used in this paper induced a moderate swelling of 19% (See Table S3 in SI).

In a final step, the HYPOP-**I** monoliths were ground and sieved into ca. 250-500 µm powders (Fig 2c). The initial polarizability of $^1$H spins in the HYPOP-**I** series was first characterized in absence of an impregnated solution to optimize the PA concentration necessary for optimum DNP conditions. In the remaining study, wet dDNP samples were obtained by slightly under-impregnating 20 mg of HYPOP-**I** powder with 60 µL of solutions.

**$^1$H polarization with HYPOPs.** DNP was performed at 7.05 T and 1.4 K in a Bruker prototype dDNP polarizer according to a standard DNP protocol described in the “methods” section. The $^1$H polarization kinetics followed a conventional first-order mono-exponential increase for all samples. Corresponding final $^1$H polarization values and build-up rates are presented in blue in Figs. 3a and 3b, respectively. A maximal $^1$H polarization of about 40 % was reached for HYPOP-**I** samples containing radicals at concentrations between 60 and 120 µmol.$g^{-1}$ while the build-up rates increased continuously with the

radical concentration. Such behavior was previously observed in HYPSO materials, which demonstrated optimal polarizations at radical concentrations between 50 and 100 µmol $g^{-1}$.[31]

After impregnation of HYPOP-**I** samples with $^{1}H$ concentrations ca. 11 mol.$L^{-1}$ ($D_2O/H_2O$/ethanol-$d_6$ mixture (8/1/1 v/v/v)), we performed DNP experiments with the same DNP protocol which led to a similar optimal PA concentration, but significantly higher maximal levels of polarization of about $P(^{1}H)$=55% (Figs. 3a and 3b in red dots). This increase in polarization to levels beyond those of dry HYPOP-**1** samples was unexpected. One possible explanation for this phenomenon would be that the PA are to some extent heterogeneously distributed across the aggregated particles forming HYPOP-**I**, some particles exhibiting a lower $^{1}H$ polarization than others and, being connected to the others through a tortuous path, are unable to polarize by long-range $^{1}H$ spin diffusion. However, once the porous polymer is impregnated with a $^{1}H$ containing solution, $^{1}H$ spin diffusion across the whole sample is strongly facilitated, which may help to reach proper hyperpolarization in all parts of the sample. In addition, the $^{1}H$ polarization kinetics diverge significantly from first-order which indicates heterogeneous build-up kinetics. This feature is typical for DNP build-up curves when polarization in the vicinity of the radicals is coupled to significant long-range spin-diffusion into radical-poor domains (the frozen solutions in our case).[27] In order to provide comparable build-up rates, the $^{1}H$ polarization kinetics were fitted with stretched exponentials

$$\mathrm{P}(^{1}H) = P_{max}\left(1 - e^{-(Rt)^{\beta}}\right),$$

with $\beta$ being the breadth of the distribution of build-up rates. The average build-up rate $R_1$ is defined as:

$$R_1 = R^{*}\frac{\beta}{\Gamma\left(\frac{1}{\beta}\right)},$$

with Γ the gamma function.[52] Both dry and impregnated matrix build-up rate follow a similar trend, albeit understandably slower for impregnated HYPOP-**I**, than for empty materials. The optimal formulation chosen for the rest of this work, HYPOP-$\mathbf{I_A}$ containing radicals at 95 µmol $g^{-1}$, provides fast and extensive $^{1}H$ polarizability to the frozen solution.

**Generating and storing $^{13}C$ hyperpolarization in HYPOP-$\mathbf{I_A}$.** The HYPOP-$\mathbf{I_A}$ sample was impregnated with a $D_2O$:ethanol (9:1 v/v) solution also including 1M [$^{13}C$]urea, 1M [1-$^{13}C$]glycine, 1M [$^{13}C$]sodium carbonate and 1M [$^{13}C$]sodium formate (four distinct target molecules) and 150 mM of sodium ascorbate. The latter is a reducing agent that readily scavenges paramagnetic oxygen in the aqueous solution as well as the PAs at the surface of the porous polymers and thus attenuates the corresponding paramagnetic relaxations.[51] The quick and efficient $^{1}H$ polarization generated in HYPOP-$\mathbf{I_A}$ and in the impregnated solution, reaching about $P(^{1}H)$ = 53% after a 2 min build-up time (Fig. 4a), is efficiently transferred to $^{13}C$ spins by $^{1}H \rightarrow ^{13}C$ multiple-contact CP[9] repeated every 4 minutes, and leads to a polarization of the $^{13}C$

target molecules of about $P(^{13}C)$ ~25 % with a 7.8 min build-up time (Fig 4b). Sequence is detailed in the methods section as well as in Section 4.2 in the SI.

Yet, the major innovation in our system does not only consists in high $^{13}C$ polarizability, but also and primarily in the extended hyperpolarization lifetime $T_1(^{13}C)$. The lifetime of $^{13}C$ polarization was assessed from the $^{13}C$ relaxation at 3.8 K and 7.05 T (Fig. 4c), monitored over 15 hours by $^{13}C$ detection with small flip angle pulses every 30 min. The pulse angle was chosen to be ~5° prevent excessive perturbation of the hyperpolarization. The relaxation time constant $T_1$ was estimated to be about 5.7 ± 0.1 h, taking into account the slight depletion of polarization due to the radiofrequency pulses (see section 8.4 in the SI).

Such a long $T_1$ relaxation time is unprecedented in the case of an arbitrary solution of target molecules and paves the way towards *transport* of hyperpolarized frozen solutions. As we previously demonstrated transport can in principle be achieved using a helium Dewar, equipped with an assembly of permanent magnets providing a moderate magnetic field (1 T).[22,27] Different strategies for fast transfers[22] have been reported, which could also be implemented in the future in combination with our approach.

**Dissolution and analysis of hyperpolarized solutions from** HYPOP-$\mathbf{I_A}$**.** Dissolution was performed by standard dDNP methods,[1] using superheated $D_2O$ (180 °C) injected directly after CP as previously described,[9] in the sample holder in the polarizer (1.4 K). The impregnated HYPOP powder was flushed out of the cryostat during the process together with the hyperpolarized solution. Therefore, an additional inline filter (See section 6 in the SI) was used to retain the HYPOP powder while letting though the melted hyperpolarized solution. The extracted hyperpolarized solution was transferred into a benchtop 80 MHz NMR apparatus (Bruker F80) equipped with a dedicated injector (Bruker BioSpin prototype), coupled to a conventional 5 mm NMR tube and ready for analysis. The whole transfer (dissolution, filtration and injection in the NMR tube) up to the start of the NMR pulse sequence took approximately 1.7 s. A magnetic tunnel[22] (4 mT solenoid) was implemented along the transfer capillary to prevent excessive polarization losses at low field, except at the position of the HYPOP filtration device (we believe that minor technological improvements solving this shortcoming may considerably increase the overall performance of the method).

After “dissolving” a solution of 0.95 M [1-$^{13}C$] sodium acetate, 0.93 M [$^{13}C$]sodium formate and 0.92 M [$^{13}C$]glycine hyperpolarized in HYPOP-$\mathbf{I_A}$, the immediate recording of $^{13}C$ spectra gave an intense $^{13}C$ spectrum (Fig 5a, 1 scan). The asymmetry of the $^{13}C$ signals indicates a substantial proton polarization of the J-coupled $^{1}Hs$.[53] Enhancement factors were calculated (see section 8.5 in the SI) to be ca. 12’000 for $^{13}C$ acetate and 6’200 for [1-$^{13}C$]-formate (i.e. 2 and 1 % absolute polarization respectively). Time-resolved $^{13}C$ spectra were measured every 5 seconds with 5 ° nutation pulses (Fig. 5b). $T_1(^{13}C)$ relaxation time constant of about 90 s for sodium acetate and of about 24 s for sodium formate were observed. These values are within the range expected for $^{13}C$ polarization in the absence of paramagnetic electron

spins[54], and demonstrate the efficient removal of HYPOP particles upon filtering. Surprisingly, $^{13}$C-glycine signals could not be observed. We believe that the $^{13}$C-glycine spins exhibited a complete relaxation in the low-field regions during transfer, most probably in the filtration system in absence of a magnetic tunnel.

The final polarization values reported here do not yet match state-of-the-art values obtained with conventional dDNP sample formulation (ca. 50 %[9]), and a lengthy work of optimization is certainly still pending. However, this work illustrates the great potential of dDNP using HYPOPs as polarization generation, storage and transport matrices which paves the way to a widespread use of dDNP in NMR or MRI experiments. Further technological improvements on the transfer line (e.g. magnetic tunnel over the whole line) still need to be implemented and may help to further increase the performance of the method.

# Conclusions

In this paper, we have demonstrated that porous polymers (HYPOP-**I**) containing TEMPO derivatives as polarizing agents and featuring a hierarchical porosity spanning from 50 nm to 1 µm can be used as multipurpose matrices for dDNP applications, with the antagonistic properties of rapidly generating 13C hyperpolarization in arbitrary aqueous mixtures, while preserving this high polarization for extended lifetimes of several hours in view of transport experiments. Together with the facile extraction of pure hyperpolarized solutions of target molecules, our strategy paves the route to a broader democratization of the use of dDNP in NMR or MRI experiments. Our strategy was illustrated with porous epoxy resins that combine straightforward synthesis and tunable morphologies, and we anticipate, that this concept of PA/target molecules separation will be further generalized to a variety of porous solids, with potentially further improved performances.

# Methods

**HYPOP synthesis & preparation.** In a falcon, Diglycidyl Ether of Bisphenol A (DGEBA), Isophorone Diamine (IPDA), Amino TEMPO were mixed with Polypropylene Glycol (PPG) as a solvent. Amount of DGEBA was calculated in order to get a ratio 2/1 with primary amines of IPDA and amino TEMPO. Quantity of amino TEMPO was calculated to reach a desired concentration taking into account the survival yield of the synthesis and the quantity of solvent was fixed at 85% of the total weight of the solution. Solutions were mixed under partial vacuum (>0,01 mbar) while stirring with a vortex. Heating the sample during this operation with a heat gun (<100 °C) can accelerate the process. Polymerization took place at 100 °C during 24 H. PPG was finally extracted by 3 exchanges with a large quantity of ethanol followed by 3 exchanges with water during at least 3 hours each before freeze-drying them. Further details of the synthesis, including effects of PPG size on porosity, are given in the section 2 in the SI. HYPOP-I monoliths are manually ground and sifted to select particles between 250 and 500 µm.

**Chemicals supply.** All chemicals used (reactants, monomers, solvents, analytes…) are currently commercially available. The list of suppliers is accessible in section 1 in the SI.

**Scanning Electron Microscopy.** Scanning Electron Microscopy experiments were performed on a ZEISS© Merlin Compact or on a Quanta© FEI 250 after deposition of 10 nm of copper using secondary electrons detectors.

**Polarizer apparatus.** All DNP measurements were performed with a prototype dDNP Polarizer developed by *Bruker Biospin*, with a helium bath cryostat operating between 1.2 K<T<4.2 K at a magnetic field of 7.05 T and equipped with $^{1}H/^{13}C$ homemade NMR probe. Microwaves were generated with a Virginia Diode system (8-20 GHz VDI synthesizer with a 198 GHz AMC amplifier / multiplier chain ). For the characterization of HYPOP, a KelF sample holder was used to reduce the $^{1}H$ signal background. For dissolution experiments, a more robust PEEK sample holder was used.

**$^{1}H$ DNP experiments.** HYPOPs where ground, and a size between 250 and 500 µm was selected using sieves. Prior to DNP experiments, HYPOP powders were used as is or impregnated with solutions to be hyperpolarized, placed in the sample cup, and inserted in the liquid helium bath of the dDNP polarizer at 4.2 K. $^{1}H$ NMR signals were measured at 3.8 K (700 mBar pressure), with 0.1° pulses every 5 seconds during 10 min until reaching the thermal equilibrium plateau. The quality factor of the $^{1}H$ NMR circuit was by attenuated by adding g a 50-Ohm resistor in series with the tuning and matching box, so as to decrease radiation-damping (potentially very intense at high polarization values) which can lead to underestimation of the polarized $^{1}H$ signal. $^{1}H$ polarization curves were recorded with at 1.4 K and 7.05 T, with the following microwave parameters: frequency of $f_{uw}$=197.648 GHz, triangular frequency modulation of width $\Delta f_{uw}$ = 160 MHz, modulation rate $f_{mod}$ = 500 Hz, and estimated power in the sample cavity $P_{uw}$ = 30 mW

**$^{13}C$ DNP experiments.** After inserting the sample, $^{13}C$ NMR signals were measured with 5° pulse every 30 min during 6 h at 3.8 K and once the plateau was reached, the thermal equilibrium NMR signal was recorded with a series of 64 pulses for improved sensitivity (See section 8.4 in the SI). The same procedure was previously applied for the measurement of the $^{13}C$ background signal (without sample). $^{1}H \rightarrow ^{13}C$ CP was performed using a 6 ms contact every 5 min to allow time for $^{1}H$ polarization to build-up and diffuse in the frozen solution in the pores of HYPOP. The CP matching condition was realized with 23 kHz $B_1$ field on both $^{1}H$ and $^{13}C$ channels (with 8 ms square pulse of $^{1}H$ (8 W) and 50.100 ramps on $^{13}C$ (150 W)). Adiabatic half passage pulses (100 kHz, 175 µs with 12 W for the $^{1}H$ channel and 150 W for the $^{13}C$ channel) were used to flip the $^{1}H$ and $^{13}C$ magnetization in the transverse plane before CP contact and to restore magnetization along z afterwards.

**Dissolution, transfer and injection experiments.** To ensure the that the fluid path does not cross a zero field, a solenoid of 1.5m length has been built around the capillary, and fed with a current of 2 A, thus generating a 4 mT all along the transfer except for the filtering system placed in close proximity to the benchtop spectrometer. 7mL of $D_2O$ solvent where pressurized at 6 Bar and heated to reach 9 Bar. After the dissolution, the HYPOP-I matrices mixed together with the molecules of interest are pushed with hot

$D_2O$ through a filtering device described in section 6 in the SI. Finally, the solution was fed into a Bruker's Prototype NMR injector directly placed in the Fourier80 benchtop NMR spectrometer.

**Hyperpolarized liquid-state NMR measurements.** Liquid-state hyperpolarized NMR spectra were measured in a Fourier 80 MHz *Bruker Biospin* benchtop spectrometer ($^1$H frequency 80.222 MHz and $^{13}$C frequency 20.1718 MHz). After injection, $^{13}$C signals were recorded every 5 s with a 5° nutation angle pulse. Final hyperpolarization enhancement was calculated by cross-calibration with a highly concentrated 3 M [1-$^{13}$C]sodium acetate reference sample, with a simple method described in detailed in section 8.5 in the SI.

# Declarations

**Data availability.** All data supporting the findings of this study are available from the corresponding author upon reasonable request.


### Acknowledgement

This research was supported by ENS-Lyon, the French CNRS, Lyon 1 University, the Institute of Chemistry at Lyon (ICL), the European Research Council under the European Union's Horizon 2020 research and innovation program (ERC Grant Agreements No. 714519 / HP4all and Marie Skłodowska-Curie Grant Agreement No. 766402 / ZULF).

The authors acknowledge Bruker BioSpin for providing the dDNP system and for their support; Venita Decker and Frank Decker from Bruker BioSpin for providing the F80 spectrometer and for their support; David Gajan, Arianna Ferrari, and Stuart J. Elliott for their assistance on the dDNP apparatus; Xiao Ji, Fanny Russel, Adrien Alonzo and Alexandra Erdmann for their synthesis work; Catherine Jose and Christophe Pages from the "service prototype" of the "*Institut des Sciences Analytiques*"; Stephane Martinez from the "*Atelier de mecanique de l'UCBL*". Emilien Etienne and Bruno Guigliarelli from the interdisciplinary French EPR network Renard at Univ. Aix. Marseille. The "Centre Technologique des Microstructures" (CTμ) for MEB images and their help with machines and Pierre-Yves Dugas for his work on microscopy.

This article is dedicated to the memory of Prof. Jean-Pierre Pascault.


### Lists of contribution

TED and DM designed and synthesized HYPOP materials. TED, LG, and DM characterized HYPOP materials. SFC, TED, OC, QC, AB, JM, and BV performed the dDNP experiments. TED, SFC, and QC analysed the DNP results. MC, JK, DE and MS designed and built the dDNP hardware. SJ designed the project and supervised the team effort. SFC, TED, SJ, and DM wrote the manuscript.

**Competing interests.** The authors declare no competing financial interests.

# References


1. Ardenkjær-Larsen, J. H. *et al.* Increase in signal-to-noise ratio of >10,000 times in liquid-state NMR. *Proc. Natl. Acad. Sci. U. S. A.* **100**, 10158–10163 (2003).
2. Zhang, G. & Hilty, C. Applications of dissolution dynamic nuclear polarization in chemistry and biochemistry. *Magn. Reson. Chem.* **56**, 566–582 (2018).
3. Lee, Y., Heo, G. S., Zeng, H., Wooley, K. L. & Hilty, C. Detection of living anionic species in polymerization reactions using hyperpolarized NMR. *J. Am. Chem. Soc.* **135**, 4636–4639 (2013).
4. Chen, H. Y., Ragavan, M. & Hilty, C. Protein folding studied by dissolution dynamic nuclear polarization. *Angew. Chemie - Int. Ed.* **52**, 9192–9195 (2013).
5. Nelson, S. J. *et al.* Metabolic imaging of patients with prostate cancer using hyperpolarized [1-$^{13}$C]pyruvate. *Sci. Transl. Med.* **5**, 198ra108 (2013).
6. Ardenkjaer-Larsen, J. H. *et al.* Dynamic nuclear polarization polarizer for sterile use intent. *NMR Biomed.* **24**, 927–932 (2011).
7. Baudin, M., Vuichoud, B., Bornet, A., Bodenhausen, G. & Jannin, S. A cryogen-consumption-free system for dynamic nuclear polarization at 9.4 T. *J. Magn. Reson.* **294**, 115–121 (2018).
8. Jannin, S., Bornet, A., Colombo, S. & Bodenhausen, G. Low-temperature cross polarization in view of enhancing dissolution Dynamic Nuclear Polarization in NMR. *Chem. Phys. Lett.* **517**, 234–236 (2011).
9. Bornet, A. *et al.* Boosting dissolution dynamic nuclear polarization by cross polarization. *J. Phys. Chem. Lett.* **4**, 111–114 (2013).
10. Miéville, P., Jannin, S., Helm, L. & Bodenhausen, G. Kinetics of yttrium-Ligand complexation monitored using hyperpolarized 89Y as a model for gadolinium in contrast agents. *J. Am. Chem. Soc.* **132**, 5006–5007 (2010).
11. Cudalbu, C. *et al.* Feasibility of in vivo15N MRS detection of hyperpolarized 15N labeled choline in rats. *Phys. Chem. Chem. Phys.* **12**, 5818 (2010).
12. Kress, T., Walrant, A., Bodenhausen, G. & Kurzbach, D. Long-Lived States in Hyperpolarized Deuterated Methyl Groups Reveal Weak Binding of Small Molecules to Proteins. *J. Phys. Chem. Lett.* **10**, 1523–1529 (2019).
13. Dumez, J. N. *et al.* Dynamic Nuclear Polarization of Long-Lived Nuclear Spin States in Methyl Groups. *J. Phys. Chem. Lett.* **8**, 3549–3555 (2017).
14. Carravetta, M. & Levitt, M. H. Long-Lived Nuclear Spin States in High-Field Solution NMR. *J. Am. Chem. Soc.* **126**, 6228–6229 (2004).
15. Carravetta, M., Johannessen, O. G. & Levitt, M. H. Beyond the T1 limit: singlet nuclear spin states in low magnetic fields. *Phys. Rev. Lett.* **92**, 153003 (2004).
16. Hu, K.-N. Polarizing agents and mechanisms for high-field dynamic nuclear polarization of frozen dielectric solids. *Solid State Nucl. Magn. Reson.* **40**, 31–41 (2011).

17. Hall, D. A. *et al.* Polarization-enhanced NMR spectroscopy of biomolecules in frozen solution. *Science* **276**, 930–932 (1997).
18. Rorschach Jr, H. E. & Rorschach, H. E. Nuclear relaxation in solids by diffusion to paramagnetic impurities. *Physica* **30**, 38–48 (1964).
19. Tse, D. & Hartmann, S. R. Nuclear spin-lattice relaxation via paramagnetic centers without spin diffusion. *Phys. Rev. Lett.* **21**, 511–514 (1968).
20. Stevens, K. W. H. The theory of paramagnetic relaxation. *Reports Prog. Phys.* **30**, 189–226 (1967).
21. Blumberg, W. E. Nuclear spin-lattice relaxation caused by paramagnetic impurities. *Phys. Rev.* **119**, 79–84 (1960).
22. Kouřil, K., Kouřilová, H., Bartram, S., Levitt, M. H. & Meier, B. *Scalable dissolution-dynamic nuclear polarization with rapid transfer of a polarized solid*. *Nature Communications* vol. 10 (2019).
23. Kouno, H. *et al.* Triplet dynamic nuclear polarization of crystalline ice using water-soluble polarizing agents. *Chem. Commun.* (2020) doi:10.1039/D0CC00836B.
24. Eichhorn, T. R. *et al.* Hyperpolarization without persistent radicals for in vivo real-time metabolic imaging. *Proc. Natl. Acad. Sci.* **110**, 18064–18069 (2013).
25. Pinon, A. C., Capozzi, A. & Ardenkjær-Larsen, J. H. Hyperpolarized water through dissolution dynamic nuclear polarization with UV-generated radicals. *Commun. Chem.* **3**, 1–9 (2020).
26. Capozzi, A., Karlsson, M., Petersen, J. R., Lerche, M. H. & Ardenkjaer-Larsen, J. H. Liquid-State 13C Polarization of 30% through Photoinduced Nonpersistent Radicals. *J. Phys. Chem. C* **122**, 7432–7443 (2018).
27. Ji, X. *et al.* Transportable hyperpolarized metabolites. *Nat. Commun.* **8**, 1–7 (2017).
28. Perez Linde, A. J. Application of cross polarisation techniques to dynamic nuclear polarisation dissolution experiments. (2010).
29. Hartmann, S. R. & Hahn, E. L. Nuclear double resonance in the rotating frame. *Phys. Rev.* **128**, 2042–2053 (1962).
30. Gajan, D. *et al.* Hybrid polarizing solids for pure hyperpolarized liquids through dissolution dynamic nuclear polarization. *Proc. Natl. Acad. Sci.* **111**, 14693–14697 (2014).
31. Cavaillès, M. *et al.* Tailored Microstructured Hyperpolarizing Matrices for Optimal Magnetic Resonance Imaging. *Angew. Chemie* **130**, 7575–7579 (2018).
32. Vuichoud, B. *et al.* Filterable Agents for Hyperpolarization of Water, Metabolites, and Proteins. *Chem. - A Eur. J.* **22**, 14696–14700 (2016).
33. Cheng, T., Mishkovsky, M., Junk, M. J. N., Münnemann, K. & Comment, A. Producing Radical-Free Hyperpolarized Perfusion Agents for In Vivo Magnetic Resonance Using Spin-Labeled Thermoresponsive Hydrogel. *Macromol. Rapid Commun.* **37**, 1074–1078 (2016).
34. Gajan, D. *et al.* Solid-phase polarization matrixes for dynamic nuclear polarization from homogeneously distributed radicals in mesostructured hybrid silica materials. *J. Am. Chem. Soc.* **135**, 15459–15466 (2013).

35. Bornet, A. *et al.* Microwave frequency modulation to enhance Dissolution Dynamic Nuclear Polarization. *Chem. Phys. Lett.* **602**, 63–67 (2014).
36. Jannin, S., Bornet, A., Melzi, R. & Bodenhausen, G. High field dynamic nuclear polarization at 6.7 T: Carbon-13 polarization above 70% within 20 min. *Chem. Phys. Lett.* **549**, 99–102 (2012).
37. Kim, Y. & Hilty, C. Affinity screening using competitive binding with fluorine-19 hyperpolarized ligands. *Angew. Chemie - Int. Ed.* **54**, 4941–4944 (2015).
38. Dumez, J.-N. *et al.* Hyperpolarized NMR of plant and cancer cell extracts at natural abundance. *Analyst* **140**, 5860–5863 (2015).
39. Khutsishvili, G. R. Spin diffusion. *Sov. Phys. Usp.* **8**, 743 (1966).
40. Yang, X.-Y. *et al.* Hierarchically porous materials: synthesis strategies and structure design. *Chem. Soc. Rev.* **46**, 481–558 (2017).
41. Wu, D. *et al.* Design and preparation of porous polymers. *Chem. Rev.* **112**, 3959–4015 (2012).
42. Hillmyer, M. A. Nanoporous materials from block copolymer precursors. *Adv. Polym. Sci.* **190**, 137–181 (2005).
43. Zhang, T., Sanguramath, R. A., Israel, S. & Silverstein, M. S. Emulsion Templating: Porous Polymers and beyond. *Macromolecules* **52**, 5445–5479 (2019).
44. Stucki, M., Loepfe, M. & Stark, W. J. Porous Polymer Membranes by Hard Templating – A Review. *Adv. Eng. Mater.* **20**, 1–18 (2018).
45. Zhao, S., Malfait, W. J., Guerrero-Alburquerque, N., Koebel, M. M. & Nyström, G. Biopolymer Aerogels and Foams: Chemistry, Properties, and Applications. *Angew. Chemie - Int. Ed.* **57**, 7580–7608 (2018).
46. Lu, W. *et al.* Porous membranes in secondary battery technologies. *Chem. Soc. Rev.* **46**, 2199–2236 (2017).
47. Traina, M., Galy, J., Gérard, J. F., Dikic, T. & Verbrugge, T. Synthesis of cross-linked epoxy microparticles: Effect of the synthesis parameters. *J. Colloid Interface Sci.* **368**, 158–164 (2012).
48. Kiefer, J., Hilborn, J. G., Månson, J. A. E., Leterrier, Y. & Hedrick, J. L. Macroporous epoxy networks via chemically induced phase separation. *Macromolecules* **29**, 4158–4160 (1996).
49. Loera, A. G., Cara, F., Dumon, M. & Pascault, J. P. Porous epoxy thermosets obtained by a polymerization-induced phase separation process of a degradable thermoplastic polymer. *Macromolecules* **35**, 6291–6297 (2002).
50. Tsujioka, N., Ishizuka, N., Tanaka, N., Kubo, T. & Hosoya, K. Well-controlled 3D skeletal epoxy-based monoliths obtained by polymerization induced phase separation. *J. Polym. Sci. Part A Polym. Chem.* **46**, 3272–3281 (2008).
51. Miéville, P. *et al.* Erratum: Scavenging free radicals to preserve enhancement and extend relaxation times in NMR using dynamic nuclear polarization (Angewandte Chemie - International Edition (2010) (49). *Angew. Chemie - Int. Ed.* **49**, 7834 (2010).
52. Johnston, D. C. Stretched exponential relaxation arising from a continuous sum of exponential decays. *Phys. Rev. B - Condens. Matter Mater. Phys.* **74**, 1–7 (2006).

53. Vuichoud, B. *et al.* Measuring absolute spin polarization in dissolution-DNP by Spin PolarimetrY Magnetic Resonance (SPY-MR) Dedicated to Stefan Schäublin, Alfred Höhener and Richard Ernst for their pioneering work. *J. Magn. Reson.* **260**, 127–135 (2015).

54. Pell, A. J., Pintacuda, G. & Grey, C. P. Paramagnetic NMR in solution and the solid state. *Prog. Nucl. Magn. Reson. Spectrosc.* **111**, 1–271 (2019).

# Figures

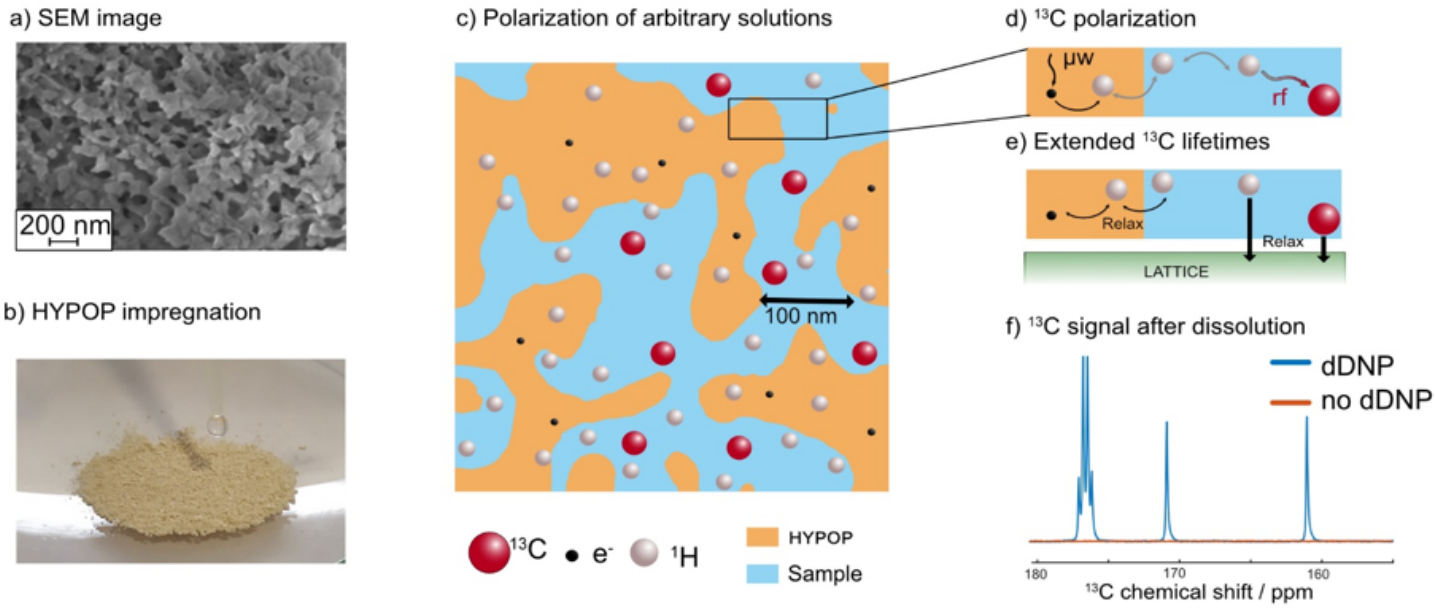


**Figure 1**

Illustration of the steps from production to extraction of transportable hyperpolarization. (a) Scanning electron microscopy of the HYPOP material used in this study. (b) Photograph of the impregnation step of powdered HYPOP. (c) Schematic representation of the porous polymer (yellow) with its PAs (black dots) impregnated with a 13C labelled molecules (red dots) in an aqueous solution (blue). 1H spins (grey dots) are abundant both in the HYPOP material and aqueous solution. (d) Schematic representation of the polarization transfer from the electrons of the PAs located within the HYPOP material to the 1H nuclei located within the HYPOP material, followed by 1H↔ 1H spin-diffusion across the material interface towards the aqueous frozen solution impregnated in the pores, and finally ended by a cross polarization (CP) transferring the 1H polarization to the 13C spins of the target molecules. (e) Schematic representation of the slow 13C nuclear spin-lattice relaxation mostly free from any paramagnetic relaxation since well physically isolated from the PAs. (f) Carbonyl region of the 13 C-NMR spectrum measured on a 80 MHz Bruker BioSpin Fourier 80 benchtop spectrometer (1 scans, 2 s), of a sample containing 0.95M [1-13C] sodium acetate, 0.93M [1-13C]sodium formate and 0.92M [1-13C]glycine, hyperpolarized with HYPOP materials, displaying a liquid-state polarization enhancement exceeding > 5000.

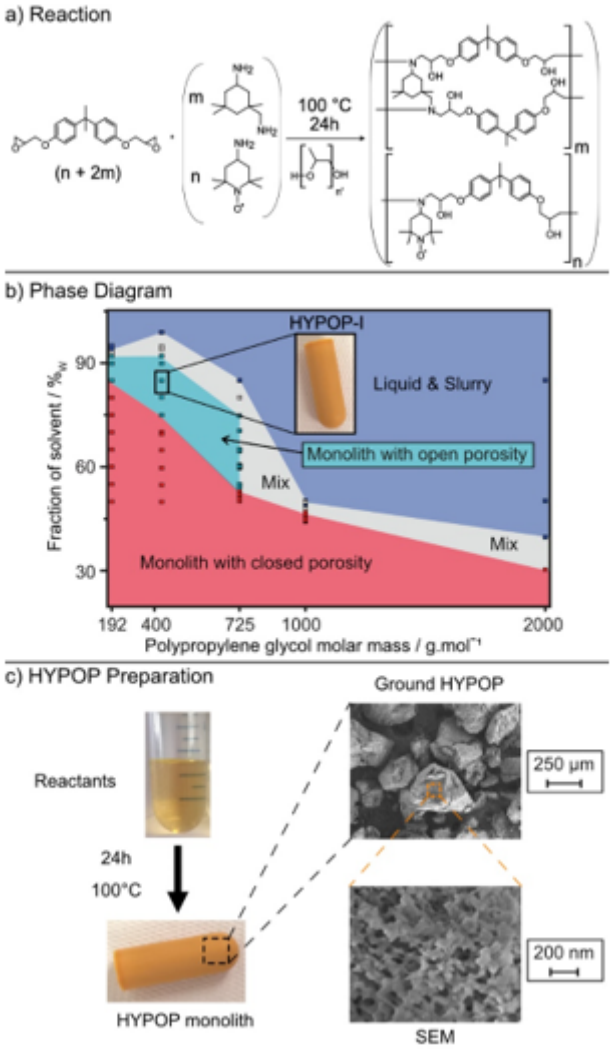


## Figure 2

a) Synthesis of TEMPO-functional and structured epoxy resins from diglycidyl ether of bisphenol A (DGEBA), isophorone diamine (IPDA) and 4-amino-TEMPO in presence of various amounts of non-reactive polypropylene glycol (PPG). b) The various morphologies obtained in absence of 4-amino-TEMPO, when varying the fraction and the average molar mass in number ($\overline{M}n$) of PPGs are reported in a phase diagram: liquids (slurry and suspensions) in dark blue, solids with closed porosity in red, heterogeneous mixtures of solids and liquids in grey and solids with open porosity in light blue. The highlighted data (85 wt% of PPG-400 g mol-1) corresponds to the HYPOP-I series (Fig 2c) that was functionalized with 4-amino-TEMPO and is reported in the remainder of the manuscript.

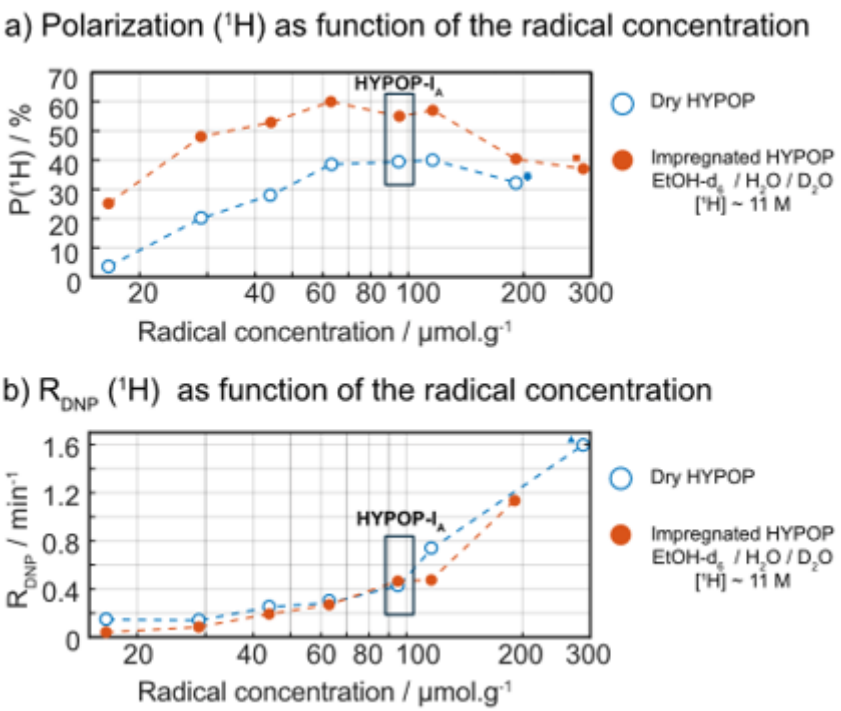


## Figure 3

1H DNP performances of the HYPOP-I series before (blue open circles) and after (red filled circles) impregnation with a solution of ethanol-d6/H2O/D2O (1/1/8 v/v/v), polarized at 1.4 K and 7.05 T, with a microwave frequency of fuw=197.648 GHz using a triangular frequency modulation of width Δfuw = ± 160 MHz and a modulation rate fmod = 500 Hz. a) steady-state 1H polarization levels and b) corresponding RDNP(1H) values. *,■,Δ Please see details in sections 8.2 & 8.3 in SI

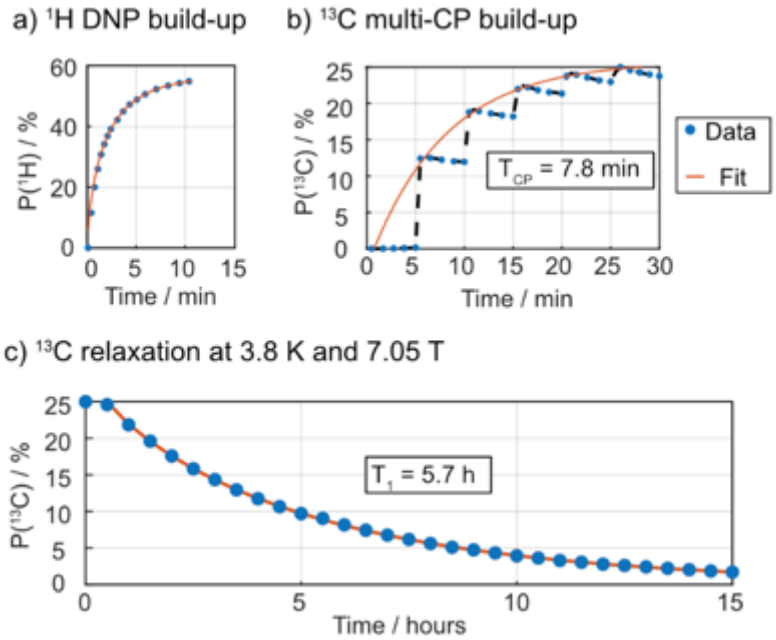


## Figure 4

a) 1H DNP build-up of HYPOP-IA sample impregnated with a solution (see in the text) measured at 1.4 K and 7.05 T, with a microwave frequency of fuw=197.648 GHz with a triangular frequency modulation of width Δfuw = ± 160 MHz and rate fmod = 500 Hz, b) Subsequent multi-CP transfer of polarization to 13C of target molecules. c) Subsequent 13C relaxation after warming the sample to 3.8 K, showing a characteristic decay constant T1(13C) = 5.7 ± 0.1 h.

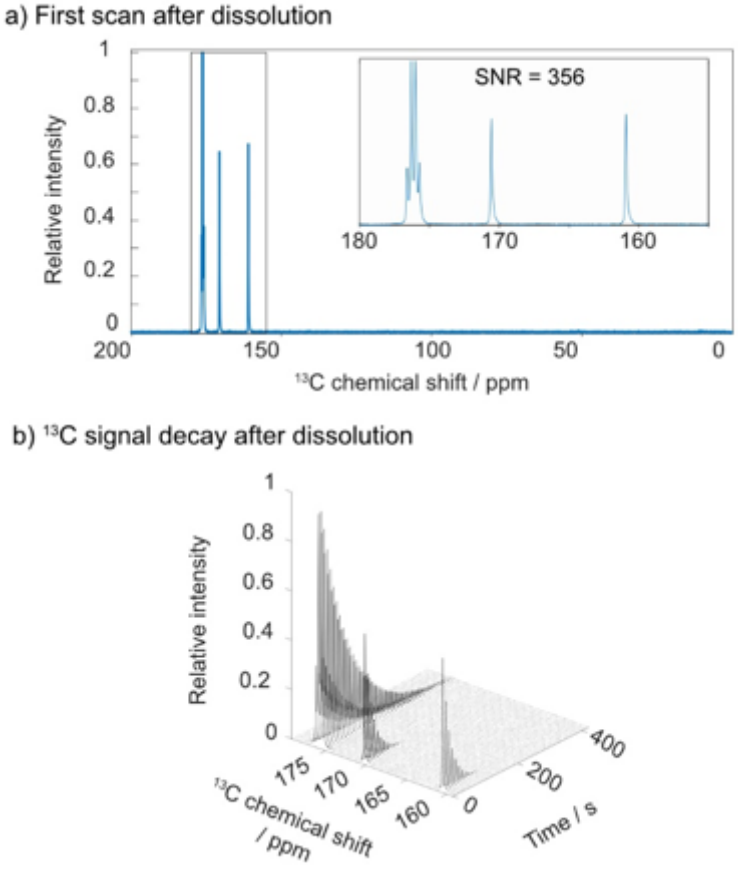


**Figure 5**

a) Full and detailed view of the first 13C spectrum b) time series of the 13C hyperpolarized spectra measured every 5 seconds with a 5° nutation angle pulse in the liquid state after hyperpolarization of a 100 µL solution of 0.9 M [1-13C]glycine at, 0.9 M [1-13C]sodium formate , 0.9 M [1-13C]sodium acetate,in 90% D2O and 10% ethanol-d6 in HYPOP-I and dissolution with 7 mL of D2O, filtration transfer and injection into a Bruker Fourier 80 benchtop NMR spectrometer (80 MHz 1H frequency).

# Supplementary Files

This is a list of supplementary files associated with this preprint. Click to download.

- HYPOPSIVF.pdf
- graphicalabstract.png